2-6-2014

Coupled Thermal and Electromagnetic Induced Decomposition in the Molecular Explosive alpha HMX; A Reactive Molecular Dynamics Study

Mitchell A. Wood
Purdue University, Birck Nanotechnology Center, wood67@purdue.edu

Adri C.T. van Duin
Penn State University

Alejandro Strachan
Purdue University, Birck Nanotechnology Center, strachan@purdue.edu

THE JOURNAL OF PHYSICAL CHEMISTRY A

Article

pubs.acs.org/JPCA

Coupled Thermal and Electromagnetic Induced Decomposition in the Molecular Explosive αHMX; A Reactive Molecular Dynamics Study

Mitchell A. Wood,[†] Adri C. T. van Duin,[‡] and Alejandro Strachan*[,†]

[†]School of Materials Engineering and Birck Nanotechnology Center, Purdue University, West Lafayette, Indiana 47907, United States

[‡]Department of Mechanical and Nuclear Engineering, Pennsylvania State University, University Park, Pennsylvania 16801, United States

Supporting Information

ABSTRACT: We use molecular dynamics simulations with the reactive potential ReaxFF to investigate the initial reactions and subsequent decomposition in the high-energy-density material α-HMX excited thermally and via electric fields at various frequencies. We focus on the role of insult type and strength on the energy increase for initial decomposition and onset of exothermic chemistry. We find both of these energies increase with the increasing rate of energy input and plateau as the processes become athermal for high loading rates. We also find that the energy increase required for exothermic reactions and, to a lesser extent, that for initial chemical reactions depend on the insult type. Decomposition can be induced with relatively weak insults if the appropriate modes are targeted but increasing anharmonicities during heating lead to fast energy transfer and equilibration between modes that limit the effect of loading type.

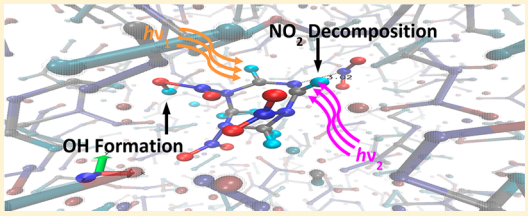

1. INTRODUCTION

The ability of high-energy-density (HED) materials to transfer energy between their various inter- and intramolecular modes of vibration and to localize energy in so-called hot spots plays a key role in the initiation of chemical reactions in these materials. Understanding energy transfer and localization mechanisms is, thus, critical to develop predictive models for their performance and safety. Energy localization not only can happen spatially but also can happen in frequency space as loading at extremely high rates can lead to nonequilibrium conditions with some modes having more than their (equilibrium) share of the total kinetic energy. For example, the translational energy in shockwaves couples predominantly to low-frequency modes, and this energy needs to be up-pumped to localized, high-frequency modes that can lead to bond-breaking.[1−7] Understanding vibrational properties of HED materials, their coupling to electromagnetic fields and energy localization/transfer mechanisms can also contribute to methods for their detection.[8−10] In this paper we use atomistic simulations to characterize the amount of energy required to initiate the decomposition and to reach the onset of exothermic chemistry of the nitramine HMX excited by a variety of insults that couple to different vibrational modes and with different strengths.

Energy localization in hotspots is responsible for the initiation of detonation in HED materials and is often responsible for accidental explosion. A wealth of experimental[10−19] and theoretical[1−4,20−28] work has been focused on identifying and quantifying the role of defects in the generation of hot spots within a shocked material. As mentioned above, energy localization not only occurs spatially but also occurs in frequency space.[10,29−33] This frequency localization and energy transfer have been studied extensively by, among others, Dlott, Moore, and McGrane with advanced spectroscopic techniques on a number of liquid[15,31,34−37] and solid phase materials.[30,38−40] In addition, the works of Coffey and others have proposed energy-transfer models that have extended the theoretical understanding of initiation in these complex materials.[41−43]

Anharmonic contributions to inter- and intramolecular vibrations in molecular materials allow for energy transfer between modes and, therefore, are important to understanding the kinetics of an excited material. The extremely fast time scales for vibron−vibron relaxation, in the 10^{-8} to 10^{-12} s range, make their experimental investigation challenging.[6,29] Dlott and co-workers measured vibron decay times of stimulated CH-stretch modes in a number of aryl−halide liquids[44] and found that relaxation times for these high-frequency modes is dependent on the density of modes in the 1000−1600 cm^{-1} range that control the decay paths down to phonon modes. Similarly, studies by McGrane and co-workers measured the lifetimes and broadening times for a large number of vibron modes in a number of energetic materials.[45,46] These results show that excited modes in HMX exhibit dephasing times ranging from 40 ps for low-frequency modes (less than 400 cm^{-1}), 20 ps in the 800−1200 cm^{-1} range, and less than 5 ps in nearly all other modes. In contrast, other materials, such as PETN and naphthalene, show dephasing times greater than 40 ps for their entire vibron frequency ranges (1−3200 cm^{-1}).[45] In addition to the work described so far, laser-driven shock experiments show great potential toward a highly repeatable and time-sensitive

Received: June 25, 2013
Revised: December 8, 2013
Published: January 8, 2014

approach for observing phonon up-pumping in a wide range of energetic and nonenergetic materials.[34,40,47,48]

In this paper we use reactive molecular dynamics (MD) simulations to characterize how chemical reactions in HMX depend on the intensity and character (e.g., the vibrational modes it couples to) of the stimulus. We study systems subjected to various heating rates and electric fields with sinusoidal time dependence of various frequencies and strengths. We find that, for fast loading rates, chemical reactions can be initiated with relatively weak insults when the stimulus couples to appropriately chosen modes. The paper is organized as follows. Section 2 provides simulation details, and section 3 shows calculations on the vibrational and infrared spectrum. Section 4 focuses on our results of HMX decomposition by direct and electric field heating and their discussion. Section 5 addresses the role of insult type on decomposition kinetics, and section 6 correlates these results to frequency-resolved energy absorption and transfer. Section 7 studies the initial chemical reactions and their dependence on insult type. Finally, conclusions are drawn in section 8.

2. SIMULATION DETAILS

A. Molecular Dynamics Simulations. We use molecular dynamics with the reactive force field ReaxFF that has been extensively used to describe HED materials.[1,2,49−53] The ReaxFF parametrization used is based on the original nitramines force field[1,2] and includes bond dissociation curves for all viable C/O/N/H single, double, and triple bonds, angle distortions for all viable C/O/N/H angular combinations, dihedral barriers, and charge distributions. Furthermore, for a number of nitramine HED materials (RDX, HMX, and PETN) full dissociation pathways, including reaction barriers, were used in the ReaxFF parameter determination. This training set was obtained from DFT calculations at the B3LYP/6-311G** and 6-31G** levels.[2] Charge equilibration parameters are obtained to reproduce partial atomic charges obtained from DFT using Mulliken populations. The original ReaxFF nitramine description[2] was nontransferable with other ReaxFF parameter sets as it did not share general or atom parameters. To remediate this, we integrated the nitramine training set with the C/H/O combustion training set, as described by Chenoweth et al.[54] For HMX, the current parameter set leads to a NO_2 dissociation energy of 41.3 kcal/mol, which is in good agreement with the DFT result (39.8 kcal/mol). The ReaxFF parameter set used in this work predicts the HONO dissociation pathway to be mildly exothermic (−9.1 kcal/mol), whereas the concerted ring-opening is more exothermic (−19.0 kcal/mol), but this latter reaction has a very substantial barrier and as such is an unlikely initiation HMX initiation pathway.

The parameters used here are fully transferable with the "combustion" ReaxFF development branch, which contains a wide number of elements,[55−58] enabling straightforward extension to, for example, metal additives. The parameter file is included in the Supporting Information.

During the MD simulations, partial atomic charges are obtained self-consistently at every time step with a conjugate gradient (CG) method with tolerance set to one part per million.[59] All simulations are carried out with the LAMMPS code[60] using a time step of 0.1 fs to integrate the equations of motion; this is sufficiently small to guarantee good energy conservation.

Direct thermal decomposition studies are performed via continuous heating using a Nose−Hoover thermostat with a coupling constant of 100 fs under isochoric conditions. After the systems reach 2000 K, we follow their subsequent decomposition using constant energy and volume simulations (*NVE* ensemble). Constant volume simulations are appropriate due to the fast heating rates in our studies.

The electric-field induced decomposition studies are performed entirely using *NVE* simulations. A field of the desired amplitude and frequency is applied to the simulation cell. The power density is computed as $\rho = (\epsilon\varepsilon_0\pi/2)E^2\omega$, where E is the amplitude of the field, ω is the frequency, and ε is the dielectric constant of HMX. These simulations are also followed by adiabatic simulations (turning the external field off) once the temperature reaches 2000 K. The field strengths were chosen such that the resulting heating rates led to decomposition time scales achievable with MD simulations and so are the rates chosen for direct heating. As a result, large electric fields are applied: from 5.6 to 35.6 × 10^8 V/m. For each target frequency, the amplitude of the field is adjusted to ensure a constant value for the calculated power density. Experimental setups used to study the laser damage on high explosives from Moore[40] used a 3 W laser confined to a spot size of approximately 200 μm on each side, which leads to power densities about one-thousand times smaller than those used in our studies. In these experiments temperature increases on the order of a few hundred Kelvin were observed over 100 s, far exceeding the time scales achievable with MD simulations. Spectroscopy techniques that measure laser-induced decomposition products use much higher pulse energies,[61,62] which can reach into the megawatt power range. These powers, if confined to a volume of 20 μm^3 would approximately match the lowest power density used in this study.

Simulating the coupling of a material with an electromagnetic field, a quantum mechanical process, via classical MD simulations necessarily leads to an approximate description. As in the quantum case, within classical mechanics the energy in the electric field is primarily absorbed by modes of the corresponding frequency and only if the mode has an associated dipole moment. Unlike the real case, our classical system absorbs energy continuously, as opposed to doing so in a quantized manner. The fact that vibrational degrees of freedom can have any amount of energy, as opposed to being quantized to values $\hbar\omega(1/2 + n)$(within the harmonic approximation), leads to an overestimation of the specific heat within classical mechanics. We note that the use of the reactive force field ReaxFF leads to an explicit description of anharmonicities in the potential energy surfaces. In addition, we ignore possible field-induced electronic excitations; as with all classical reactive MD simulations, we assume the electrons remain in their ground state throughout the process. Thus, processes such as dielectric breakdown are beyond the capability of the current MD simulations. Despite these approximations, our simulations provide interesting insight into how the manner in which energy is inputted into a reactive molecular crystal affects its response.

B. Systems of Interest. The α phase of HMX exhibits an orthorhombic unit cell containing eight molecules. An input structure with 2 × 1 × 4 α-HMX unit cells resulting in 64 molecules (1792 atoms) is used in our simulations. Periodic boundary conditions are imposed along all directions leading to a defect-free perfect single crystal.

C. Simulation Analysis. Particularly important for this study is the spectral analysis of our samples. The power spectrum measures the kinetic energy density as a function of frequency and is obtained from the Fourier transformation of time-dependent atomic velocities:[63]

$$P(\omega) = \frac{\beta\tau}{N}\sum_{j=1}^{3N} mj\left|\sum_{n=0}^{N-1} vj(n\Delta t)e^{-i2\pi\omega n\Delta t}\right|^2 \quad (1)$$

where $v_j(t)$ are the atomic velocities at time t, β is defined as $(k_BT)^{-1}$ with T being the temperature, τ is the sampling period, m_j is the mass of atom j, Δt is the sampling rate, and N is the number of frames to be analyzed. Our implementation uses a fast Fourier transform to solve eq 1. The vibrational density of states can be obtained by dividing eq 1 by $1/2k_BT$ under thermal equilibrium conditions, where every vibrational mode should have $1/2k_BT$ of kinetic energy. A subset of these vibrations is infrared (IR) active, and this can be determined by tracking the dipole moments over time. We compute the IR spectra from the Fourier transform of the time derivative of the total dipole moment in the simulation as shown in eq 2, where $\bar{M}$ is defined as $\bar{M}(i) = \Sigma_{j=1}^{N} q_j(i)\, v_j(i)$, with $q_j(i)$ and $v_j(i)$ representing the charge and velocity of atom j at sampling frame i, respectively.[64]

$$I(\omega) = \frac{2\pi\omega}{3\hbar cn}(1 - e^{-\beta\hbar\omega})\sum_{n=0}^{N-1} e^{-i2\pi\omega n\Delta t}\left[\frac{1}{M-j}\sum_{i=1}^{M-j}\dot{M}(i)\cdot\dot{M}(i+j)\right] \quad (2)$$

3. VIBRATIONAL DENSITY OF STATES AND IR SPECTRA

Figure 1 shows the calculated vibrational and infrared spectra for α-HMX under ambient conditions. We used a 50-ps-long MD trajectory with a sampling rate of 3 fs, yielding a spectral window of 0−5000 cm^{-1} (0−150 THz) with a frequency resolution of 1.36 cm^{-1} for the vibrational spectrum and 2.72 cm^{-1} for the IR spectrum. To obtain good statistics in the autocorrelation function calculation, we compute it up to a time corresponding to half of the total simulation time. The dashed vertical bars in Figure 1b divide the spectra into frequency regions that will be used in section 5B.

The ReaxFF IR spectrum is in good overall agreement with experiments even though the potential was not tuned for vibrational accuracy. We observe a slight blue shift in the spectra; for example, the carbon−hydrogen symmetric and asymmetric stretch modes are known experimentally[65] to lie around 2950 cm^{-1} whereas we calculate them out as far as 3250 cm^{-1}. However, the relative peak positions and contributing elements agree with previous experimental and theoretical studies.[65,66] Normal mode enumeration[67] was not undertaken in this study, though a comparable nonreactive force field[68] that was parametrized for vibrational accuracy was used for direct comparison of the power spectrum shown in Figure 1a.

4. THERMAL AND ELECTRIC FIELD INDUCED DECOMPOSITION AND REACTION

A. Thermal-Induced Decomposition. In the thermal-induced decomposition simulations we heat an α-HMX sample to 2000 K with a thermostat and at zero pressure, after which adiabatic simulations (*NVE* ensemble) are performed to follow the subsequent reactions. The heating rates were chosen to span both those observed experimentally for high explosives under critical shock loading (10−25 K/ps) and those that have been observed under laser driven shock experiments at high powers (50 K/ps and above).[23,36,69]

Figure 2 shows the results of these direct heated cases with rates in the range 10−100 K/ps. The simulations of the reaction kinetics of HMX under constant heating rates are used as a baseline for the laser heated cases. The potential energy per molecule uses the perfect crystal as a reference (−2571.492 kcal/mol $molecule^{-1}$)

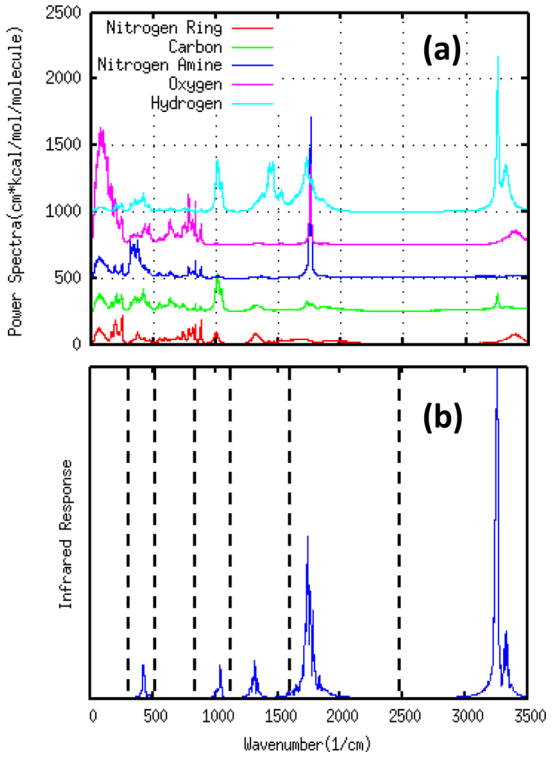

Figure 1. (a) Calculated vibrational spectrum of α-HMX at 300 K from molecular dynamics with the ReaxFF interatomic potential. Peak contributions by element type are offset vertically for clarity. (b) Infrared spectrum of α-HMX at 300 K calculated from the same trajectory used in the top panel.

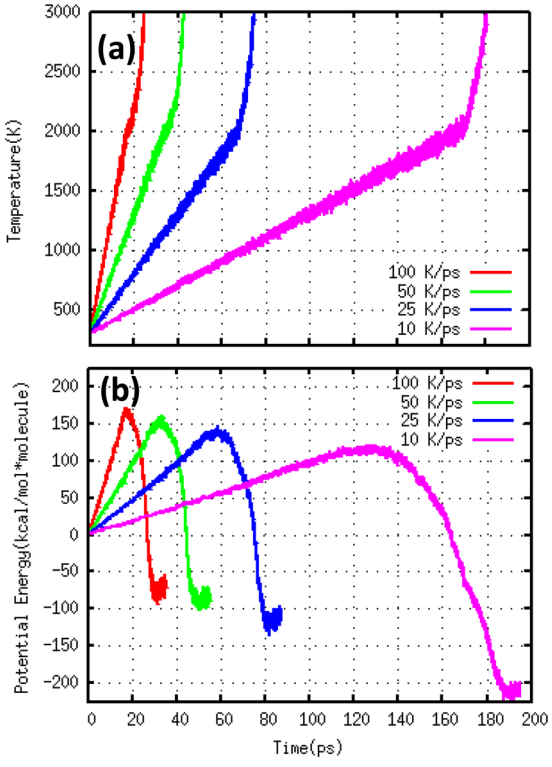

Figure 2. (a) Temperature of α-HMX over time in the canonical (*NVT*) ensemble while being ramped at various rates from 300 to 2000 K, after which simulation is run in the microcanonical ensemble (*NVE*). (b) Potential energy of the same system in the top panel. Values are zeroed on the initial configuration of the crystal at 300 K.

dx.doi.org/10.1021/jp406248m | J. Phys. Chem. A 2014, 118, 885−895

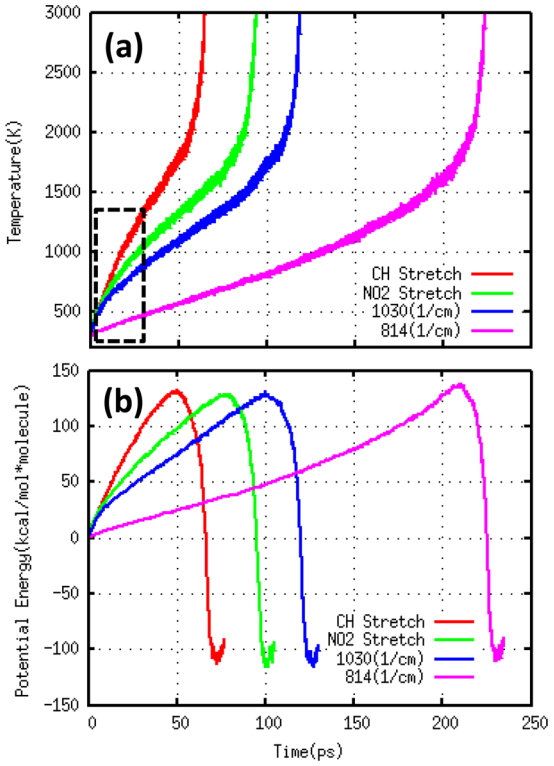

Figure 3. (a) Temperature of α-HMX over time in the microcanonical (*NVE*) ensemble under laser insult at varying frequencies for 1.604 μW/nm^3. (b) Potential energy of the same system in the top panel. Values are zeroed on the initial configuration of the crystal at 300 K.

at room temperature and ambient pressure. As an additional validation of both the reactive potential and the simulation method for direct heating, we performed a Kissinger analysis of the potential energy and temperature evolution from these simulations.[73,77] We used the temperature corresponding to the onset of exothermic reactions and preset heating rates in a Kissinger plot to extract an activation energy of 23.529 kcal/mol; see Figure S1 in the Supporting Information. This value is comparable to the activation energy of 35 kcal/mol extracted by Henson and collaborators from a wide range of experiments[78] and those in prior MD studies[2] of RDX, a HED nitramine similar HMX.

The increase in the rate of heating after the thermostated stage, Figure 2a, is due to the exothermic reactions of HMX; this can be observed in the decrease in potential energy seen in Figure 2b. We observe the beginning of exothermic reactions during the heating stage but its onset depends on the heating rate. Increasing the heating rates leads to larger potential energies before exothermic reactions start decreasing the potential energy. In other words, fast heating rates lead to higher potential energy before exothermic reactions. Note that higher potential energies are achieved in the reacted material for the faster heating rates because the thermostat needs to add more energy to take the system to 2000 K; for slower rates, the exothermic reactions contribute more to the heating up to 2000 K. This is an artifact of our simulation setup.

B. Electric Field-Induced Decomposition. We chose four frequencies to study the response of α-HMX to electromagnetic radiation; these frequencies are chosen on the basis of the spectral analysis in section 3. Three frequencies are selected to couple with IR-active moments: 3254 cm^{-1} (97.62 THz, CH stretch), 1765 cm^{-1} (52.95 THz, NO_2 stretch), and 1030 cm^{-1} (30.9 THz). The fourth frequency, 814 cm^{-1} (24.42 THz), corresponds to a low-frequency mode with no significant IR activity. Due to the capability of the atomic charges to redistribute, it is possible to have a mode without an IR moment to couple with an electric field, as long as the external field can cause some amount of polarization in the material.

In the simulations represented in Figure 3 electric fields with a power density of 1.604 μW/nm^3 at the various frequencies are applied to the samples. Figure 3a shows the time evolution of the temperature and Figure 3b of potential energy. As in the thermal-induced decomposition studies, the insult is turned off once the samples reach a temperature of 2000 K and the subsequent dynamics is described with constant energy MD. Our simulations show different regimes of energy absorption leading to different heating rates.

We are interested in understanding the energy transfer from the electric field to the sample, and Figure 4a shows the temperature evolution during the initial stages. These results indicate a two-stage heating process: (i) At short time scales, fields that couple to an IR mode of the material lead to rapid heating. As will become apparent in section 5B, during this stage the material is away from thermal equilibrium and we will denote this process nonequilibrium heating. (ii) The second stage is marked by a decrease in the heating rate (see the change in slopes in Figure 4a); this stage will be called steady-state heating. The decrease in the coupling is due to the target modes (and the vibrational peaks in general) becoming broader

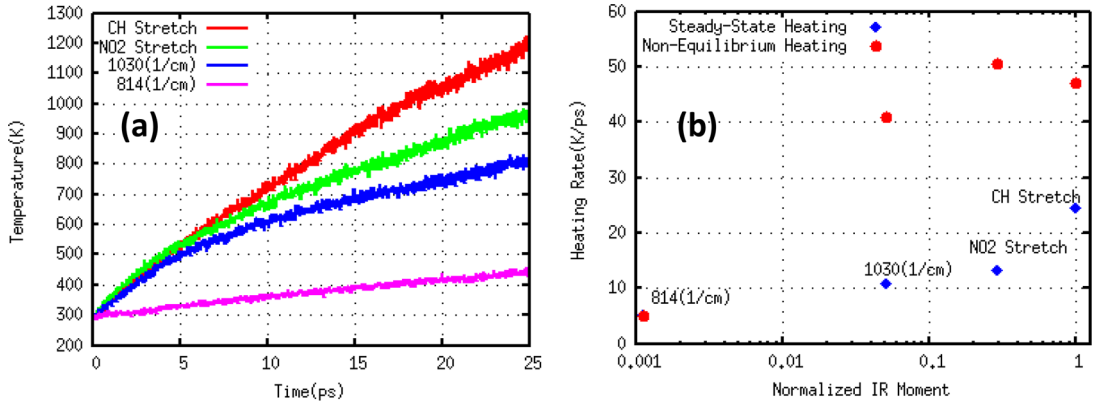

Figure 4. (a) Enhanced version of the temperature vs time plot shown in Figure 3a (dashed box). (b) Heating rates observed from α-HMX under laser insult targeting various vibrational modes at 1.604 μW/nm^3. The IR moments on the horizontal axis were calculated at 300 K and zero pressure.

dx.doi.org/10.1021/jp406248m | J. Phys. Chem. A 2014, 118, 885−895

with increasing temperature. Broadening of peaks leads to weaker coupling with the harmonic electric field and the steady-state heating rates show less dependence on frequency than the initial rates. Note that the simulation corresponding to 814 cm^{-1} (where there is no IR active mode) exhibits only stage two. To identify how much these modes broaden and shift with increasing temperature, the vibrational density of states (vDOS) is plotted in Figure 5 for αHMX for temperatures in the range

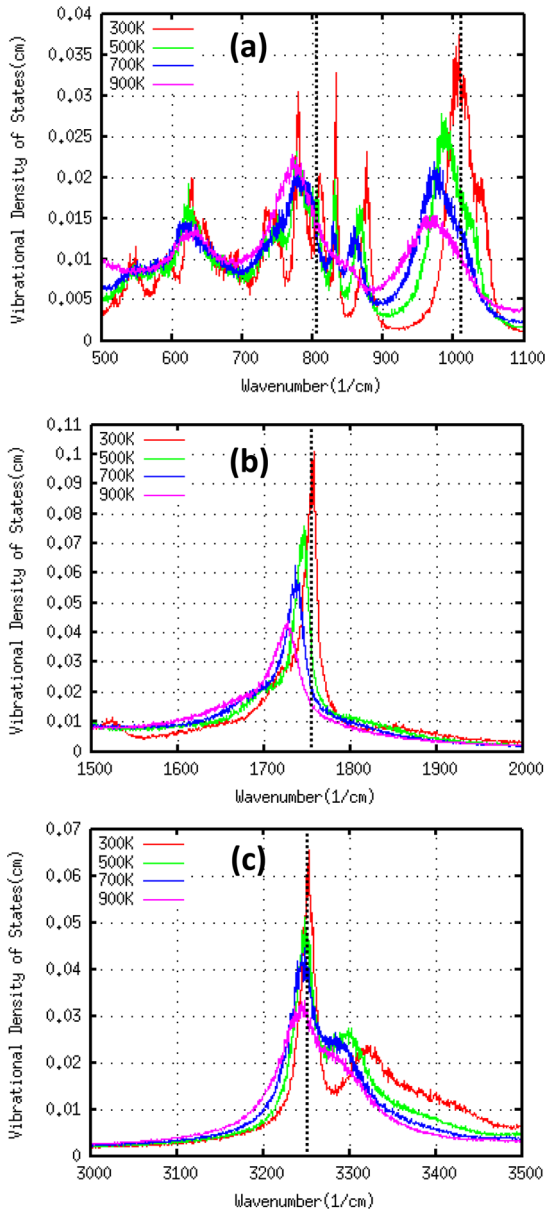

Figure 5. Vibrational density of states for α-HMX for a range of temperatures around the transition between nonequilibrium and steady-state heating. To keep all series on the same ordinate scale, the density of states is used rather than the power spectrum as in Figure 1a. Dashed lines indicate the frequencies used for electric-field driven simulations.

300−900 K. In each panel of Figure 5, a dashed line marks the frequency of the electric field. Comparing the vibrational peak positions to the excitation frequency, we see how the red shifts affect the efficient absorption from the electric field insult. In no case is the shift in frequency enough to negate coupling with the field. The closest to this extreme case is the NO_2 stretch mode, which shifts by approximately 30 cm^{-1} from 300 to 900 K but is still observed to maintain strong coupling at high temperatures, as seen from Figure 3a.

The results in Figures 4 and 5 provide a qualitative verification of our simulations coupling electric fields and reactive MD simulations. We find the expected correlation between heating rate and oscillator strength of the target mode. In addition, the effects of the anharmonic coupling between modes and its temperature dependence can be seen. Of interest for the reactive model is how these anharmonic couplings preferentially heat the material and how this electromagnetic insult will differ from direct heating.

5. ROLE OF INSULT TYPE AND MAGNITUDE ON CHEMICAL KINETICS AND ENERGETICS

The simulations described in section 4 were expanded upon and carried out for six direct heating rates ranging from 5 to 200 K/ps and five power densities ranging from 1.604 to 16.04 $\mu W/nm^3$. Simulations for each of the four target modes outlined previously were carried out for all five laser power densities, giving us an equally wide scope of heating rates from the electromagnetic insult as the direct heating simulations. We now focus on the analysis of the role of insult type and rate of energy increase on chemical reactions.

A. Initial Decomposition. To characterize the effect of insult type and magnitude on the initial chemical decomposition, we track the time evolution of the number of HMX molecules. Figure 6a shows the decrease in the number of HMX molecules as decomposition occurs. As will be discussed below, the initial reactions involve NO_2 loss followed closely by OH, HONO, and H_2O formation. This sequence of molecules, however, is liable to be altered with high-power-density insults, as will be shown in section 7. To set a standard across all simulations, we define the time for initial decomposition as that when the population of HMX molecules is reduced to three-fourths of its original value. We are interested in the amount of energy in the material when initial decomposition is achieved for the various insults. Thus, we define the energy increase for initial chemistry ($\Delta\varepsilon_{init}$) as the increase in potential energy from the initial, ground-state energy (at T = 300 K), to the one corresponding to the time where one-fourth of the initial HMX molecules have decomposed. Figure 6b shows $\Delta\varepsilon_{init}$ as a function of heating rate for the various cases studied. The values of $\Delta\varepsilon_{init}$ were averaged over ten independent simulations for each electric field strength and frequency combination. Our MD results indicate that the amount of energy required for initial decomposition depends strongly on insult type and the rate at which energy is inputted into the HED material. Regardless of insult character, we find that higher rates of energy input lead to higher values of $\Delta\varepsilon_{init}$; these changes in rate can almost double the $\Delta\varepsilon_{init}$. This is somewhat expected, as fast coupling tends to overshoot thermally activated processes. For fast enough heating, the process is assumed to become athermal wherein the $\Delta\varepsilon_{init}$ plateaus at a maximum value. This limiting $\Delta\varepsilon_{init}$ of approximately 150 kcal/mol per HMX molecule can be compared with the energy associated with NO_2 dissociation ~41 kcal/mol in the gas phase and the activation energy of 23.529 kcal/mol calculated from the Kissinger analysis in section 4.

More interesting is the observation that the energy required to induce decomposition is strongly dependent on insult type. Figure 6b shows that electromagnetic coupling to high-frequency modes responsible for the initial chemical reactions

dx.doi.org/10.1021/jp406248m | J. Phys. Chem. A 2014, 118, 885−895

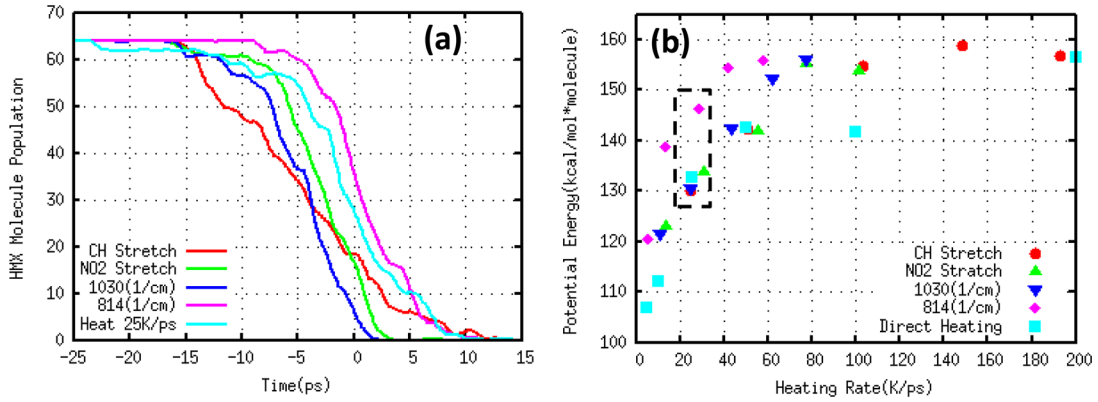

Figure 6. (a) HMX population for insult strengths resulting in a heating rate near 25 K/ps. The simulations for these population curves have their corresponding points bound by a dashed box in Figure 6b. The time scale has a reference ($t = 0$) to the onset of exothermic chemistry. (b) Potential energy change from the perfect crystal value for one-quarter decomposition of HMX molecules as a function of heating rate for all insult types, obtained from an ensemble average over ten independent simulations.

leads to decomposition with $\Delta\varepsilon_{init}$ approximately the same as directly heated samples. On the other hand, if the electromagnetic field couples to low-frequency modes decomposition requires significantly more energy (greater change in potential energy). This effect is most notable in the range of heating rates between 20 and 60 K/ps where a collection of field driven samples at 814 cm^{-1} show significantly higher $\Delta\varepsilon_{init}$ than the directly heated samples.

Interestingly, we find that the population of HMX molecules remaining at the onset of exothermic chemistry depends strongly on the insult type (Figure 6a). Note that the time axis in the figure is referenced to the time corresponding to the onset of exothermicity for each condition (each time is determined with an accuracy of approximately 1 ps across ten simulations). Targeting high-frequency modes results in smaller HMX populations at the time exothermicity is first observed. Strong electromagnetic fields can result in additional changes in initial chemistry as will be shown in section 7.

B. Exothermic Reactions. We now turn our attention to whether the insult type has an effect on the onset of exothermic chemistry. The maximum in potential energy (Figures 2 and 3) defines an energy increase for the onset exothermic chemistry ($\Delta\varepsilon_{exo}$). Figure 7 shows $\Delta\varepsilon_{exo}$ as a function of heating rate for all insults studied (electric fields at different frequencies and temperatures). The energy increase is measured from the ground state of the crystal, and a dashed line fitted to the direct heating simulation results is included to guide the eye. As with the initial chemical reactions, $\Delta\varepsilon_{exo}$ increases with increasing heating rate. The $\Delta\varepsilon_{exo}$ for direct heating is similar to those associated with electromagnetic insults targeted at modes that can initiate chemical reactions, but with a thermostat each vibration is given the same amount of energy.

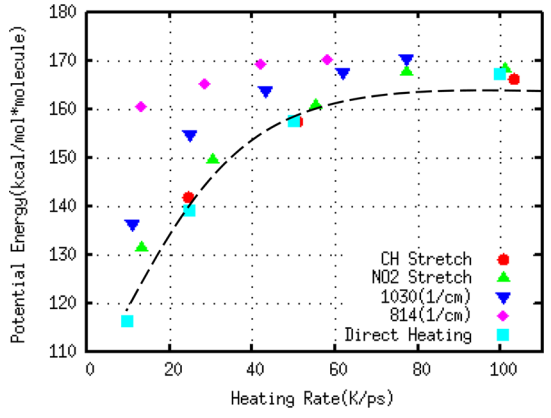

Figure 7. Maximum potential energy achieved as the system is heated plotted against the strength of the insult. Values are not absolute, but energy input is above the common starting structure at 300 K.

When the low-frequency, IR-inactive mode at 814 cm^{-1} is targeted, more energy input is required to trigger the initial endothermic reactions. This result indicates that energy transfer from such low-frequency modes to higher frequency ones responsible for chemical reactions remains weak even after the initial chemical decomposition occurs. It is interesting to note that the rate limiting step in shock-induced detonation is the up-pumping of energy from low-frequency phonons to high-frequency vibrons; our results indicate that under such conditions the effective internal energy increase for exothermic chemistry may be quite a bit higher than the one associated with thermal initiation.

6. FREQUENCY-RESOLVED ENERGY INPUT AND TRANSFER

Thus far, our results have shown that the manner in which energy is inputted into an energetic material affects the onset of decomposition and exothermic reactions. To understand these observed trends, we now focus on the spectral energy content in the material as a function of insult frequency. Figure 8 shows the kinetic energy content in the frequency regions marked in Figure 1b as a function of time for the four different target modes at a power density of 1.604 $\mu W/nm^3$. Spectra were calculated using a 10 ps sampling window with frames every 3 fs for both laser and direct heated samples. The spectra are then broken down into seven distinct, sequential, frequency ranges that are then integrated over to give the amount of kinetic energy contained in that particular region of frequencies. These values of kinetic energy will continuously increase with time as long as the insult is present, but the amount and rates at which they change will differ depending on the insult type. For direct comparison, we normalize each frequency region by the amount of kinetic energy observed in a comparable direct heated case. This corrects for peaks that broaden or shift across the preset regions as the temperature is increased. As closely as possible, given the discrete sampling window, we match the heating rate and temperature of the electric field driven

dx.doi.org/10.1021/jp406248m | J. Phys. Chem. A 2014, 118, 885−895

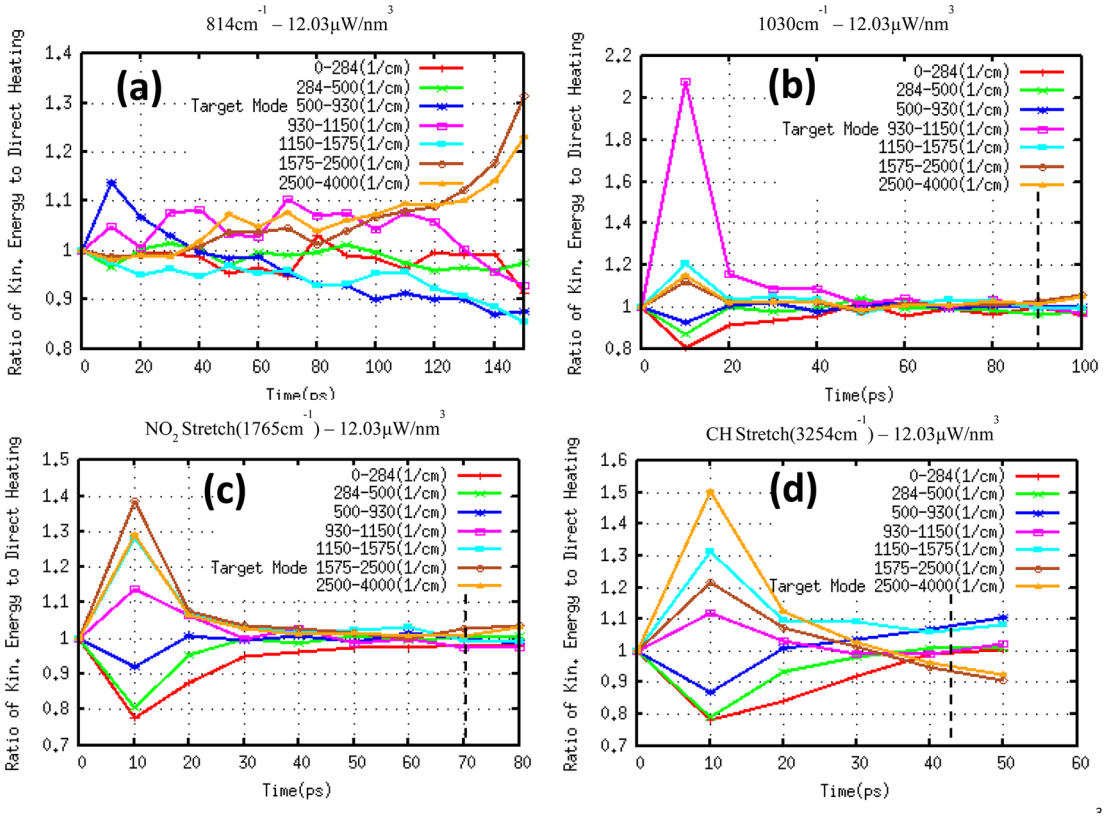

Figure 8. Energy localization plots for the four laser targeted modes of α-HMX at a power density of 27.86 μW (1.604 μW/nm^3). (a) Insult targeting the mode at 814 cm^{-1}. (b) Insult targeting the mode at 1030 cm^{-1}. (c) Insult targeting the NO_2 Stretch mode. (d) Insult targeting the CH stretch mode. The vertical axis for all four plots is the integrand of the laser heated vibrational spectra normalized by a comparable heating rate and temperature of a direct heated sample. A value of unity refers to equal energy distribution seen from direct heating.

simulations to a calculated spectra from a directly heated sample. For example, if the observed heating rate in an electric field heated study is 14 K/ps with a temperature around 1000 K we will choose from the appropriate 10 ps window of the 10 K/ps directly heated sample that is closest to this temperature. This process also allows us to correct for the initial high heating rates observed with laser heated samples. Once these spectra are paired, each integrating region is normalized, yielding values close to unity. Therefore, in this analysis, a value of unity is an energy distribution from the field driven samples that matches that of direct heating and can be considered as an equilibrium state of the system.

With the exception of Figure 8a, each plot in Figure 8 is terminated when the potential energy maxima have been reached (that is at the beginning of overall exothermic reaction) and the vertical dashed lines indicate the 1/4 decomposition mark. Figure 8 also shows that each of the four electric fields will initially preferentially heat up modes close to its target mode. In the first 10 ps, there are noticeable differences in the magnitude of energy localization at the target mode that varies from a 15% change in energy in the 814 cm^{-1} target mode up to 210% increase over direct heating as seen in the target mode at 1030 cm^{-1}. In the two highest frequency target modes, NO_2 (Figure 8c) and CH stretch (Figure 8d), the localization of energy in the target mode is also accompanied by other modes of lower frequency being excited. This suggests significant coupling between these sets of molecular modes. In all cases except the one corresponding to 814 cm^{-1}, there is an initial excitation and successive relaxation through modes in the range of 1150−1575 cm^{-1} (light blue series in Figure 8a−d); this range of frequencies is dominated by contributions from hydrogen, carbon and nitrogen on the ring of HMX. This observation suggests that these modes are responsible for the coupling of high-frequency modes to the lower frequency, molecular deformation modes. It is also worth noticing in Figure 8a that the energy distribution becomes less uniform at later times. We attribute this to the loss of high-frequency modes in the directly heated spectrum used to normalize these results due to chemical reactions. Thus, the lack of chemical events in the system excited at 814 cm^{-1} at the same temperature as a directly heated sample results in the apparent increase of energy stored in these high-frequency modes. This result further supports our claim that there are inefficient energy-transfer mechanisms from low- to high-frequency vibrons, in agreement with previous work on vibron relaxation and multiphonon up pumping.[41,42]

The intramolecular vibrational energy-transfer rates in HMX have been observed to be much faster than in other HE materials.[46] This rapid energy transfer between molecular modes and subsequently to the phonon bath brings the material into equilibrium with the insult on very short time scales. As a result, low-power-density insults cannot heat the material up to decomposition temperatures in the time scales of vibrational energy transfer. However, the decomposition kinetics can be altered if higher power density fields are used, as will be shown in section 7.

7. ROLE OF INSULT TYPE AND ENERGY INCREASE RATE ON CHEMICAL REACTIONS

We now focus our attention to whether the insult type affects the initial chemical reactions. Using the results discussed in

dx.doi.org/10.1021/jp406248m | J. Phys. Chem. A 2014, 118, 885−895

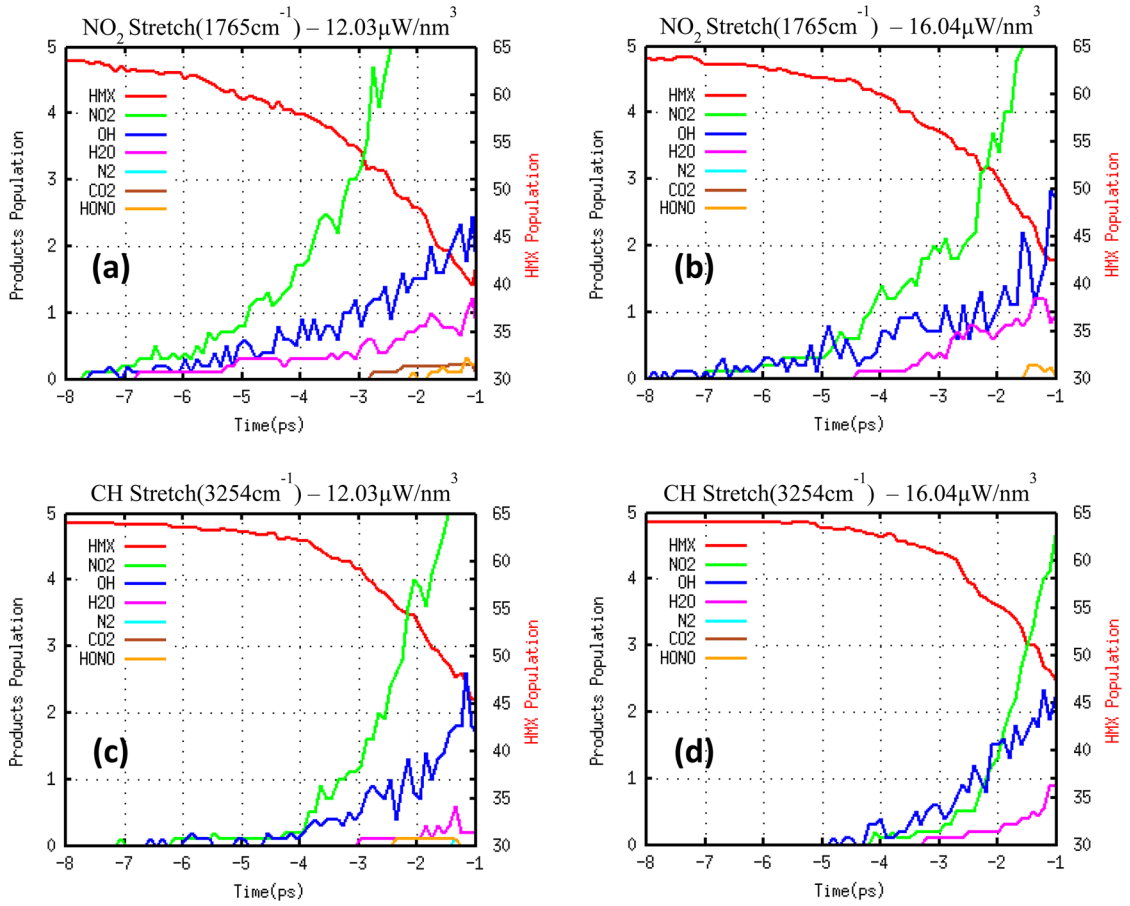

Figure 9. Changes in initial chemistry observed with high-power-density fields targeting the NO_2 and CH stretch modes, respectively. Time scales are set such that at zero the potential energy of the system is at its maximum (exotherm onset). Two laser powers are shown for each target mode to show the switch from NO_2 to OH and H_2O formation. Fractional values of molecule populations are allowed because each plot has the molecule populations averaged over ten independent simulations to reduce noise.

Figure 8 as a guide, we now move to much higher power density electric fields and study the resulting molecules formed from this nonequilibrium energy distribution of energy among the vibrons in α-HMX. Figure 9a–d shows the time evolution of the population of small products and intermediate molecules as well as HMX during electric field heating. The time in these plots is measured from the beginning of exothermic reaction (maximum in potential energy). Consistent with previous atomistic studies[26,50,70] we identify NO_2 and OH, in that order, as the first molecules to form from both low-power-density field driven samples and directly heated samples. This is also in agreement with experimental observations.[71,72] Example molecule population analyses for a pair of directly heated α-HMX samples are given in the Supporting Information, Figures S2(a,b) and S3(a,b). Changes in the initial steps of decomposition in α-HMX under electric field insult are shown in Figure 9. In Figure 9, (a) and (b) correspond to fields with frequency matching the NO_2 stretch mode whereas (c) and (d) show the results from targeting the CH stretch mode.

To display the initial chemical events clearly, the HMX populations over time are displayed on the right y-axis and the populations of the product molecules are displayed on the left. Each plot in Figure 9 has the data averaged over ten independent runs, thus allowing for fractional values of the molecule population. Figure 9a,b shows that the HMX population has dropped by about half from its starting value at the exotherm onset with NO_2, OH, and H_2O molecules being formed in that order for both power densities shown. Despite the fluctuations intrinsic to atomistic simulations our results show that targeting the NO_2 modes with high-strength fields favors the early formation of NO_2 molecules and at a larger time interval between the initial decomposition and the onset of exothermic reactions as compared to the CH stretch excitation. Conversely, at the highest power densities tested matching the CH stretch frequency we see an earlier onset of the OH population rise, along with the reversal of the first two chemical species identified during decomposition. This can be seen in Figure 9c,d where the rise of OH and H_2O are seen earlier, and even before, the rise of NO_2 molecules.

8. DISCUSSION AND CONCLUSIONS

In summary, we performed extensive MD simulations of decomposition of the HED material HMX with the reactive potential ReaxFF. We induce decomposition either with electric fields (of various frequencies) or via direct heating. We characterized the energy input into the material as a function of frequency for the various electric fields and found nonequilibrium conditions and a two-stage process when IR-active modes are targeted. Furthermore, the simulations show that the character and strength of the insult affects the energy increase required for initial chemistry and for the onset of exothermic chemical reactions. Furthermore, for high-strength fields the initial chemical reactions are affected by the selected target mode. We find that fields with frequencies matching

dx.doi.org/10.1021/jp406248m | J. Phys. Chem. A 2014, 118, 885–895

high-frequency modes can lead to decomposition with significantly less overall energy input in regards to similar field-driven samples at lower frequencies.

These results displaying changes in the initial chemical events that depend on the character of the insult are very reminiscent of work done by Bunker and Hase[74,75] into the non-RRKM reaction kinetics of gas phase molecules. RRKM behavior implies that prior to reaction the material will explore all available states, including those leading to the reaction, and achieve local equilibrium. Figures 8 and 9 indicate that high-strength electric fields can lead to a nonequilibrium distribution of energy among vibron modes and can, in turn, result in non-RRKM behavior.[74−76] Additional work connecting nonequilibrium reactive MD simulations with non-RRKM behavior would, in our view, contribute to a deeper understanding of nonequilibrium chemical reactions in the condensed phase and improve the interpretation of the simulations. The results presented in this paper contribute to a deeper understanding of chemical reactions in high-energy-density materials and can lead to a more detailed understanding of detonation and accidental initiation. Additional work into the mechanisms and time scales for energy localization and the role of defects as well as extending these studies to other materials would be critical to develop a complete picture of chemical initiation in HED materials.

■ ASSOCIATED CONTENT

Supporting Information

Kissinger plot for simulations heated using a Nose−Hoover thermostat. Graphcs of decomposition time for products. ReaxFF parameter set used in this work. This information is available free of charge via the Internet at http://pubs.acs.org.

■ AUTHOR INFORMATION

Corresponding Author

*A. Strachan: e-mail, Strachan@purdue.edu.

Notes

The authors declare no competing financial interest.

■ REFERENCES

(1) Strachan, A.; van Duin, A. C. T.; Chakraborty, D.; Dasgupta, S.; Goddard, W. A. Shock waves in high-energy materials: The Initial Chemical Events in Nitramine RDX. *Phys. Rev. Lett.* **2003**, *91*, 4.

(2) Strachan, A.; Kober, E. M.; van Duin, A. C. T.; Oxgaard, J.; Goddard, W. A. Thermal Decomposition of RDX From Reactive Molecular Dynamics. *J. Chem. Phys.* **2005**, *122*, 05402.

(3) Holian, B. L.; Germann, T. C.; Maillet, J. B.; White, C. T. Atomistic Mechanism for Hot Spot Initiation. *Phys. Rev. Lett.* **2002**, *89*, 4.

(4) Jaramillo, E.; Sewell, T. D.; Strachan, A. Atomic-Level View of Inelastic Deformation in a Shock Loaded Molecular Crystal. *Phys. Rev. B* **2007**, *76*, 6.

(5) An, Q.; Zybin, S. V.; Goddard, W. A.; Jaramillo-Botero, A.; Blanco, M.; Luo, S. N. Elucidation of the Dynamics for Hot-Spot Initiation at Nonuniform Interfaces of Highly Shocked Materials. *Phys. Rev. B* **2011**, *84*, 5.

(6) Chen, S.; Tolbert, W. A.; Dlott, D. D. Direct Measurement of Ultrafast Multiphonon Up-Pumping in High Explosives. *J. Phys. Chem.* **1994**, *98*, 7759−7766.

(7) Tokmakoff, A.; Fayer, M. D.; Dlott, D. D. Chemical-Reaction Initiation and Hot-Spot Formation in Shocked Energetic Molecular Materials. *J. Phys. Chem.* **1993**, *97*, 1901−1913.

(8) Ye, S.; Tonokura, K.; Koshi, M. Vibron Dynamics in RDX, beta-HMX and Tetryl Crystals. *Chem. Phys.* **2003**, *293* (1), 1−8.

(9) Fried, L. E.; Ruggiero, A. J. Energy-Transfer Rates in Primary, Secondary, and Insensitive Explosives. *J. Phys. Chem.* **1994**, *98*, 9786−9791.

(10) Hong, X. Y.; Chen, S.; Dlott, D. D. Ultrafast Mode-Specific Intermolecular Vibrational-Energy Transfer To Liquid Nitromethane. *J. Phys. Chem.* **1995**, *99*, 9102−9109.

(11) Dlott, D. D. Thinking Big (and Small) About Energetic Materials. *Mater. Sci. Technol.* **2006**, *22*, 463−473.

(12) Kuklja, M. M. On The Initiation Of Chemical Reactions By Electronic Excitations In Molecular Solids. *Appl. Phys. A: Mater. Sci. Process.* **2003**, *76*, 359−366.

(13) Ahmad, S. R.; Russell, D. A. Laser Ignition of Pyrotechnics - Effects of Wavelength, Composition and Confinement. *Propellants Explosives Pyrotechnics* **2005**, *30*, 131−139.

(14) Ahmad, S. R.; Russell, D. A. Studies into Laser Ignition of Confined Pyrotechnics. *Propellants Explosives Pyrotechnics* **2008**, *33*, 396−402.

(15) Seong, N.-H.; Fang, Y.; Dlott, D. D. Vibrational Energy Dynamics of Normal and Deuterated Liquid Benzene. *J. Phys. Chem. A* **2009**, *113*, 1445−1452.

(16) Shigeto, S.; Pang, Y.; Fang, Y.; Dlott, D. D. Vibrational Relaxation of Normal and Deuterated Liquid Nitromethane. *J. Phys. Chem. B* **2008**, *112*, 232−241.

(17) Yu, H.; Hambir, S. A.; Dlott, D. D. Ultrafast Dynamics Of Nanotechnology Energetic Materials. In *Multifunctional Energetic Materials*; Thadhani, N. N., Armstrong, R. W., Gash, A. E., Wilson, W. H., Eds.; MRS Symposium Proceedings; MRS: Warrendale, PA, 2006; Vol. *896*, pp 71−79.

(18) Armstrong, R. W.; Ammon, H. L.; Elban, W. L.; Tsai, D. H. Investigation Of Hot Spot Characteristics In Energetic Crystals. *Thermochim. Acta* **2002**, *384*, 303−313.

(19) Mares, J. O.; Miller, J. K.; Sharp, N. D.; Moore, D. S.; Adams, D. E.; Groven, L. J.; Rhoads, J. F.; Son, S. F. Thermal and Mechanical Response of PBX 9501 Under Contact Excitation. *J. Appl. Phys.* **2013**, *113*, 084904.

(20) Xiao, J.; Zhao, L.; Zhu, W.; Chen, J.; Ji, G.; Zhao, F.; Wu, Q.; Xiao, H. Molecular Dynamics Study on the Relationships of Modeling, Structural and Energy Properties With Sensitivity For RDX-Based PBXs. *Science China-Chemistry* **2012**, *55*, 2587−2594.

(21) Xiao, J. J.; Wang, W. R.; Chen, J.; Ji, G. F.; Zhu, W.; Xiao, H. M. Study on Structure, Sensitivity and Mechanical Properties of HMX and HMX-Based PBXs With Molecular Dynamics Simulation. *Comput. Theor. Chem.* **2012**, *999*, 21−27.

(22) Xiao, J. J.; Li, S. Y.; Chen, J.; Ji, G. F.; Zhu, W.; Zhao, F.; Wu, Q.; Xiao, H. M. Molecular Dynamics Study on the Correlation Between Structure and Sensitivity For Defective RDX Crystals and Their PBXs. *J. Mol. Model.* **2013**, *19*, 803−809.

(23) Dlott, D. D.; Hambir, S.; Franken, J. The New Wave in Shock Waves. *J. Phys. Chem. B* **1998**, *102*, 2121−2130.

(24) Kuklja, M. M.; Rashkeev, S. N. Modeling Defect-Induced Phenomena. *Static Compression of Energetic Materials* **2008**, 291−326.

(25) Rice, B. M.; Sorescu, D. C.; Kabadi, V.; Agrawal, P. M.; Thompson, D. L. Molecular Simulations of Dynamic Processes of Solid Explosives. *Transformational Science and Technology for the Current and Future Force* **2006**, *42*.

(26) Zhou, T.-T.; Huang, F.-L. Effects of Defects on Thermal Decomposition of HMX via ReaxFF Molecular Dynamics Simulations. *J. Phys. Chem. B* **2011**, *115*, 278−287.

(27) Cawkwell, M. J.; Sewell, T. D.; Zheng, L.; Thompson, D. L. Shock-Induced Shear Bands in an Energetic Molecular Crystal: Application of Shock-Front Absorbing Boundary Conditions to Molecular Dynamics Simulations. *Phys. Rev. B* **2008**, *78*, 014107.

(28) Menikoff, R.; Sewell, T. D. Constituent Properties of HMX Needed for Mesoscale Simulations. *Combust. Theor. Model.* **2002**, *6*, 103−125.

(29) Chen, S.; Hong, X. Y.; Hill, J. R.; Dlott, D. D. Ultrafast Energy-Transfer in High Explosives - Vibrational Cooling. *J. Phys. Chem.* **1995**, *99*, 4525−4530.

(30) Deak, J. C.; Iwaki, L. K.; Dlott, D. D. Vibrational Energy Redistribution in Polyatomic Liquids: Ultrafast IR-Raman Spectroscopy of Acetonitrile. *J. Phys. Chem. A* **1998**, *102*, 8193−8201.
(31) Dlott, D. D. Vibrational Energy Redistribution in Polyatomic Liquids: 3D Infrared-Raman Spectroscopy. *Chem. Phys.* **2001**, *266*, 149−166.
(32) Kim, H.; Dlott, D. D. Molecular-Dynamics Simulation Of Nanoscale Thermal Conduction And Vibrational Cooling In A Crystalline Naphthalene Cluster. *J. Chem. Phys.* **1991**, *94*, 8203−8209.
(33) Aluker, E. D.; Krechetov, A. G.; Mitrofanov, A. Y.; Zverev, A. S.; Kuklja, M. M. Understanding Limits of the Thermal Mechanism of Laser Initiation of Energetic Materials. *J. Phys. Chem. C* **2012**, *116*, 24482−24486.
(34) Dang, N. C.; Bolme, C. A.; Moore, D. S.; McGrane, S. D. Shock Induced Chemistry in Liquids Studied With Ultrafast Dynamic Ellipsometry and Visible Transient Absorption Spectroscopy. *J. Phys. Chem. A* **2012**, *116*, 10301−10309.
(35) Carter, J. A.; Wang, Z.; Lagutchev, A.; Fang, Y.; Seong, N.-H.; Cahill, D. G.; Dlott, D. D. Ultrafast Shock Wave Coherent Dissociation and Spectroscopy Of Materials. APS-SCCM, Waikoloa, HI, Jun 24−29, 2007.
(36) Conner, R. W.; Dlott, D. D. Time-Resolved Spectroscopy of Initiation and Ignition of Flash-Heated Nanoparticle Energetic Materials. *J. Phys. Chem. C* **2012**, *116*, 14737−14747.
(37) Iwaki, L. K.; Dlott, D. D. Three-dimensional Spectroscopy of Vibrational Energy Relaxation in Liquid Methanol. *J. Phys. Chem. A* **2000**, *104*, 9101−9112.
(38) Moore, D. S.; Schmidt, S. C. Vibrational Spectroscopy Of Materials Under Extreme-Pressure And Temperature. *J. Mol. Struct.* **1995**, *347*, 101−111.
(39) Hare, D. E.; Franken, J.; Dlott, D. D. A New Method For Studying Picosecond Dynamics Of Shocked Solids - Application To Crystalline Energetic Materials. *Chem. Phys. Lett.* **1995**, *244*, 224−230.
(40) McGrane, S. D.; Moore, D. S. Continuous Wave Laser Irradiation of Explosives. *Propellants Explosives Pyrotechnics* **2011**, *36*, 327−334.
(41) McNesby, K. L.; Coffey, C. S. Spectroscopic Determination of Impact Sensitivities of Explosives. *J. Phys. Chem. B* **1997**, *101*, 3097−3104.
(42) Coffey, C. S.; Sharma, J. Plastic Deformation, Energy Dissipation, and Initiation of Crystalline Explosives. *Phys. Rev. B* **1999**, *60*, 9365−9371.
(43) Namkung, J.; Coffey, C. S. Plastic Deformation Rate and Initiation Of Crystalline Explosives. APS-SCCM, Atlanta, GA, 2002; pp 1003−1006.
(44) Pein, B. C.; Seong, N.-H.; Dlott, D. D. Vibrational Energy Relaxation of Liquid Aryl-Halides X-C6H5 (X = F, Cl, Br, I). *J. Phys. Chem. A* **2010**, *114*, 10500−10507.
(45) McGrane, S. D.; Shreve, A. P. Temperature-Dependent Raman Spectra of Triaminotrinitrobenzene: Anharmonic Mode Couplings in an Energetic Material. *J. Chem. Phys.* **2003**, *119*, 5834−5841.
(46) McGrane, S. D.; Barber, J.; Quenneville, J. Anharmonic Vibrational Properties of Explosives from Temperature-Dependent Raman. *J. Phys. Chem. A* **2005**, *109*, 9919−9927.
(47) Brown, K. E.; Shaw, W. L.; Zheng, X.; Dlott, D. D. Simplified Laser-Driven Flyer Plates for Shock Compression Science. *Rev. Sci. Instrum.* **2012**, *83*, 103901.
(48) Brown, K. E.; Fu, Y.; Shaw, W. L.; Dlott, D. D. Time-Resolved Emission of Dye Probes in a Shock-Compressed Polymer. *J. Appl. Phys.* **2012**, *112*, 103508.
(49) Zhang, L. Z.; van Duin, A. C. T.; Zybin, S. V.; Goddard, W. A. Thermal Decomposition of Hydrazines from Reactive Dynamics Using the ReaxFF Reactive Force Field. *J. Phys. Chem. B* **2009**, *113*, 10770−10778.
(50) Zhang, L. Z.; Zybin, S. V.; van Duin, A. C. T.; Dasgupta, S.; Goddard, W. A.; Kober, E. M. Carbon Cluster Formation during Thermal Decomposition of Octahydro-1,3,5,7-tetranitro-1,3,5,7-tetrazocine and 1,3,5-Triamino-2,4,6-trinitrobenzene High Explosives from ReaxFF Reactive Molecular Dynamics Simulations. *J. Phys. Chem. A* **2009**, *113*, 10619−10640.
(51) Zhang, L.; Zybin, S. V.; Van Duin, A. C. T.; Goddard, W. A. Modeling High Rate Impact Sensitivity of Perfect RDX and HMX Crystals by ReaxFF Reactive Dynamics. *Journal of Energetic Materials* **2010**, *28*, 92−127.
(52) Rom, N.; Zybin, S. V.; van Duin, A. C. T.; Goddard, W. A.; Zeiri, Y.; Katz, G.; Kosloff, R. Density-Dependent Liquid Nitromethane Decomposition: Molecular Dynamics Simulations Based on ReaxFF. *J. Phys. Chem. A* **2011**, *115*, 10181−10202.
(53) Zybin, S. V.; Goddard, W. A., III; Xu, P.; van Duin, A. C. T.; Thompson, A. P. Physical Mechanism of Anisotropic Sensitivity in Pentaerythritol Tetranitrate From Compressive-Shear Reaction Dynamics Simulations. *Appl. Phys. Lett.* **2010**, *96*, 081918.
(54) Chenoweth, K.; van Duin, A. C. T.; Goddard, W. A. ReaxFF Reactive Force Field for Molecular Dynamics Simulations of Hydrocarbon Oxidation. *J. Phys. Chem. A* **2008**, *112*, 1040−1053.
(55) Castro-Marcano, F.; van Duin, A. C. T. Comparison of Thermal and Catalytic Cracking of 1-heptene From ReaxFF Reactive Molecular Dynamics Simulations. *Combust. Flame* **2013**, *160*, 766−775.
(56) Neyts, E. C.; Khalilov, U.; Pourtois, G.; van Duin, A. C. T. Hyperthermal Oxygen Interacting with Silicon Surfaces: Adsorption, Implantation, and Damage Creation. *J. Phys. Chem. C* **2011**, *115*, 4818−4823.
(57) Salmon, E.; van Duin, A. C. T.; Lorant, F.; Marquaire, P. M.; Goddard, W. A. Thermal Decomposition Process in Algaenan of Botryococcus Braunii Race L. Part 2: Molecular Dynamics Simulations Using The Reaxff Reactive Force Field. *Org. Geochem.* **2009**, *40*, 416−427.
(58) Chenoweth, K.; van Duin, A. C. T.; Dasgupta, S.; Goddard, W. A. Initiation Mechanisms and Kinetics of Pyrolysis and Combustion of JP-10 Hydrocarbon Jet Fuel. *J. Phys. Chem. A* **2009**, *113*, 1740−1746.
(59) Rappe, A. K.; Goddard, W. A. Charge Equilibration for Molecular-Dynamics Simulations. *J. Phys. Chem.* **1991**, *95*, 3358−3363.
(60) Plimpton, S. Fast Parallel Algorithms For Short-Range Molecular-Dynamics. *J. Comput. Phys.* **1995**, *117*, 1−19.
(61) De Lucia, F. C.; Harmon, R. S.; McNesby, K. L.; Winkel, R. J.; Miziolek, A. W. Laser-induced Breakdown Spectroscopy Analysis of Energetic Materials. *Appl. Opt.* **2003**, *42*, 6148−6152.
(62) Waterbury, R. D.; Pal, A.; Killinger, D. K.; Rose, J.; Dottery, E. L.; Ontai, G. Standoff LIBS Measurements of Energetic Materials Using a 266nm Excitation Laser. 9th Annual Conference for Chemical, Biological, Radiological, Nuclear, and Explosives (CBRNE) Sensing, Orlando, FL, Mar 18−20, 2008.
(63) Berens, P. H.; Mackay, D. H. J.; White, G. M.; Wilson, K. R. Thermodynamics and Quantum Corrections From Molecular-Dynamics for Liquid Water. *J. Chem. Phys.* **1983**, *79*, 2375−2389.
(64) Boulard, B.; Kieffer, J.; Phifer, C. C.; Angell, C. A. Vibrational-Spectra In Fluoride-Crystals And Glasses At Normal And High-Pressures By Computer-Simulation. *J. Non-Cryst. Solids* **1992**, *140*, 350−358.
(65) Brand, H. V.; Rabie, R. L.; Funk, D. J.; Diaz-Acosta, I.; Pulay, P.; Lippert, T. K. Theoretical and Experimental Study of the Vibrational Spectra of the alpha, beta, and delta Phases of Octahydro-1,3,5,7-tetranitro-1,3,5,7-tetrazocine (HMX). *J. Phys. Chem. B* **2002**, *106*, 10594−10604.
(66) Zhu, W.; Xiao, J.; Ji, G.; Zhao, F.; Xiao, H. First-principles Study of the Four Polymorphs of Crystalline Octahydro-1,3,5,7-tetranitro-1,3,5,7-tetrazocine. *J. Phys. Chem. B* **2007**, *111*, 12715−12722.
(67) Pravica, M.; Galley, M.; Kim, E.; Weck, P.; Liu, Z. A Far- and Mid-Infrared Study of HMX (octahydro-1,3,5,7-tetranitro-1,3,5,7-tetrazocine) Under High Pressure. *Chem. Phys. Lett.* **2010**, *500*, 28−34.
(68) Smith, G. D.; Bharadwaj, R. K. Quantum Chemistry Based Force Field for Simulations of HMX. *J. Phys. Chem. B* **1999**, *103*, 3570−3575.
(69) Yang, Y. Q.; Sun, Z. Y.; Wang, S. F.; Dlott, D. D. Fast Spectroscopy of Laser-Initiated Nanoenergetic Materials. *J. Phys. Chem. B* **2003**, *107*, 4485−4493.

(70) Chakraborty, D.; Muller, R. P.; Dasgupta, S.; Goddard, W. A. A Detailed Model for the Decomposition of Nitramines: RDX and HMX. *J. Comput.-Aided Mater. Des.* **2002**, *8*, 203−212.
(71) Adams, G. F.; Shaw, R. W. Chemical-Reactions in Energetic Materials. *Annu. Rev. Phys. Chem.* **1992**, *43*, 311−340.
(72) Behrens, R.; Bulusu, S. Thermal-Decomposition of Energetic Materials 0.2. Deuterium-Isotope Effects and Isotopic Scrambling in Condensed-Phase Decomposition of Octahydro-1,3,5,7-Tetranitro-1,3,5,7-Tetrazocine. *J. Phys. Chem.* **1991**, *95*, 5838−5845.
(73) Orava, J.; Greer, A. L.; Gholipour, B.; Hewak, D. W.; Smith, C. E. Characterization of Supercooled Liquid Ge2Sb2Te5 and its Crystallization by Ultrafast-Heating Calorimetry. *Nat. Mater.* **2012**, *11*, 279−283.
(74) Bunker, D. L.; Hase, W. L. Non-RRKM Unimolecular Kinetics - Molecules in General, and CH3NC in Particular. *J. Chem. Phys.* **1973**, *59*, 4621−4632.
(75) Bunker, D. L.; Wright, K. R.; Hase, W. L.; Houle, F. A. Exit-Channel Coupling Effects in the Unimolecular Decomposition Of Triatomics. *J. Phys. Chem.* **1979**, *83* (8), 933−936.
(76) Viswanathan, R.; Raff, L. M.; Thompson, D. L. Monte-Carlo Transition-State Theory - CH4- CH3+H, SiH-4- SiH-3+H. *J. Chem. Phys.* **1984**, *81*, 828−832.
(77) Kissinger, H. E. Variation of Peak Temperature With Heating Rate in Differential Thermal Analysis. *J. Res. Natl. Bur. Std.* **1956**, *57*, 217−221.
(78) Henson, B. F.; Asay, B. W.; Smilowitz, L. B.; Dickson, P. M. Ignition chemistry in HMX from thermal explosion to detonation. APS-SCCM, Atlanta, GA, Jun 24−29, 2001; American Institute of Physics: Atlanta, GA, 2001; pp 1069−1072.